HERA Results

Katerina Müller, Hanno Perrey, Thomas Schörner-Sadenius

Jet production measurements at HERA allow detailed tests of our understanding of perturbative QCD. The concepts of factorization, of the perturbative expansion of the cross section and of PDF universality can all be tested. In addition, the strong coupling constant, α_s, can be extracted from HERA jet production data. A further issue of particular relevance to the LHC, is the possible effects of multi-parton interactions and the underlying event. At HERA, such effects can be studied in resolved photoproduction events, since the hadronic structure of the photon means that photon-proton collisions are similar, in some respects, to hadron-hadron collisions.

The production of isolated photons, produced directly in the hard interaction, also provides a very sensitive probe of perturbative QCD, since the photons are largely insensitive to the effects of hadronisation. A good understanding of the Standard Model production mechanism of isolated photons is also important for searches of new particles decaying to photons at hadron colliders (eg. $H \rightarrow \gamma\gamma$).

In this section, some recent HERA measurements of both jet production (mainly in the photoproduction regime), and of isolated photons, are reviewed. In addition, some recent measurements sensitive to the effects of multi-parton interactions and the underlying event are discussed.

1 HERA results on jets and prompt photons in photoproduction

Authors: Hanno Perrey, Thomas Schörner-Sadenius

In photoproduction at HERA, a quasi-real photon emitted from the incoming electron collides with a parton from the incoming proton. In such events, hadronic jets and also prompt (meaning: radiated by one of the outgoing quarks) photons can be produced. The photoproduction of hadronic jets can be classified into two types of processes in leading-order (LO) QCD: direct and resolved. In direct processes, the entire photon and its momentum participate in the hard scatter (left side of Fig. 1), while resolved processes involve a photon acting as a source of quarks and gluons, with only a photon momentum fraction x_γ participating in the hard scatter (right side of Fig. 1). It is due to the presence of resolved events that HERA data might be useful for further constraining the photon PDFs.

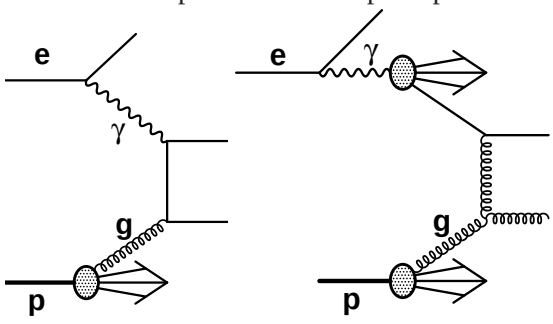

Fig. 1: Feynman diagrams of direct and resolved dijet photoproduction at leading order.

This contribution presents a review of some recent results on jet (and prompt photon) photoproduction at HERA. Some emphasis is placed on the prospects of using such measurements to constrain the proton and the photon PDFs. In addition, some results on multi-parton

interactions and the underlying event are briefly summarised. It should be pointed out that most of these results use data only from the HERA-I data taking period, such that an improvement in statistical precision is to be expected by making use of all available data.

1.1 The concept of the resolved photon

Fig. 1 shows Feynman diagrams for direct (left) and resolved (right) photoproduction of di-jets. Statistically, direct events are dominated by quark propagators whereas resolved events are mostly characterized by gluon propagators. This difference should lead to a distinctly different angular behaviour of the final-state jets: whereas the quark propagator (quarks being spin-$1/2$ particles) should lead to a distribution in the cosine of the centre-of-mass scattering angle, $\cos\theta^*$, like $(1-|\cos\theta^*|)^{-1}$, in the gluon case a distribution like $(1-|\cos\theta^*|)^{-2}$ is expected. In other words, the cross section of the resolved part is expected to rise more rapidly towards higher $\cos\theta^*$ than that of the direct part. Fig. 2 shows the experimental evidence [1]: the dijet cross section as a function of $\cos\theta^*$ for a direct-enriched (left) and a resolved-enriched data sample (right). It is obvious that the above predictions are fulfilled, the resolved distribution rising much more rapidly than the direct one. These distributions thus form an important test of the concept of the resolved photon. Similar results have also been obtained by the ZEUS collaboration [2].

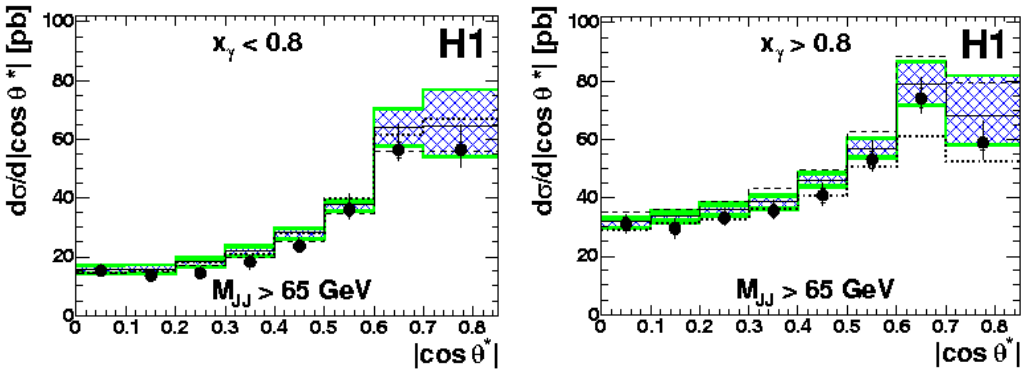

Fig. 2: Photoproduction dijet cross section as function of centre-of-mass scattering angle, $\cos\theta^*$, for direct- (left) and resolved-enriched (right) samples [1].

In the above discussion, the distinction between direct and resolved data samples has been made. On the theoretical side, this distinction is meaningful only at LO. On the experimental side, the distinguishing observable x_γ is not directly accessible but has to be reconstructed from the two final-state jets in much the same way as the proton's momentum fraction x_p entering the hard scattering,

$$x_\gamma = \frac{E_{T,1}e^{-\eta_1} + E_{T,2}e^{-\eta_2}}{2yE_e}, \qquad x_p = \frac{E_{T,1}e^{+\eta_1} + E_{T,2}e^{+\eta_2}}{2E_p},$$

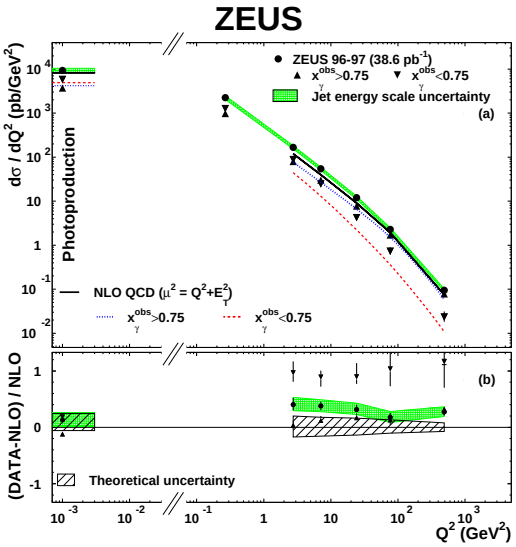

Fig. 3: Fraction of resolved events as a function of Q^2 [3].

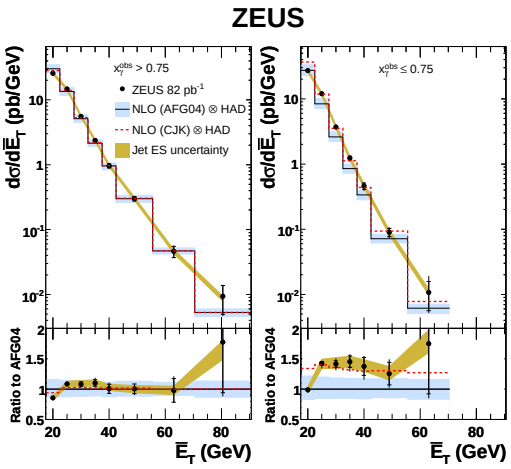

Fig. 4: Photoproduction dijet cross sections as functions of the mean transverse jet energy, $\overline{E}_T$, for a direct- and a resolved enriched sample [4].

where $E_{T,i}$ and η_i are the jet transverse energies and pseudorapidities, y is the inelasticity (characterizing the energy loss of the scattered electron) and E_e and E_p are the electron and proton beam energies. Typically, the resolved regime is defined to comprise values of x_γ between 0 and 0.75 or 0.8.

Note, however, that the phenomenon of the resolved photon is not strictly confined to the photoproduction regime. Also, the virtual photon entering into deep inelastic scattering events can exhibit a hadronic substructure, leading to a resolved contribution to DIS. The ZEUS collaboration has evaluated the fraction of resolved events in both photoproduction and DIS, measuring the fraction of dijet events with x_γ below and above 0.75. The results are shown in Fig. 3, as a function of the photon virtuality Q^2 [3], and are compared to NLO QCD calculations. It is found that even at large Q^2 values (highly virtual photons), there is a significant contribution from resolved events and that for DIS this component of the data is not correctly described by the QCD predictions (which do not include any resolved photon option). In contrast, the resolved contribution to photoproduction is well described by NLO QCD.

1.2 Jet cross sections in photoproduction

Numerous measurements of inclusive-jet, dijet and multijet cross sections have been performed by the HERA experiments. A very recent result [4] is presented in Fig. 4, which shows the dijet cross section as a function of the mean dijet transverse energy, $\overline{E}_T$, for a sample enhanced in direct and a sample enhanced in resolved events. The measurements are compared to an NLO QCD prediction using two different parameterisations of the photon PDFs.

The data in the direct regime are especially well described by the theory (on the level of 10% or better), as can be seen in the bottom left part of the figure, which shows the ratio of data over NLO prediction. The uncertainties here are dominated by the theoretical uncertainty which is of the order of 15%. The situation in the resolved regime is slightly more complicated and will be discussed in some more detail below.

Many more examples of photoproduction jet cross sections and their successful description by NLO QCD exist. Fig. 6 [1] shows the dijet cross section as a function of x_p in different regions of x_γ and jet pseudorapidity. Both the momentum fractions and the pseudorapidity distributions of the jets are sensitive to the momentum distributions of partons inside the proton, making these measurements important tests of QCD. It can be seen again that the data are very well described by NLO QCD, on the level of 10%, which are well covered by the combined uncertainties. Only for large x_p values, with both jets going forward ($\eta_{1,2} > 1$), do some deviations between data and theory occur (see Fig. 6, bottom right). These differences might be explained by the large uncertainties on the proton PDFs for large momentum fractions.

Fig. 5 [4] shows, for the same data sample as in Fig. 4, the cross section as a function of the mean jet pseudorapidity, $\overline{\eta}$. The data are again shown separately for direct- and resolved-enhanced samples and are compared to NLO QCD predictions using different parameterisations of the photon PDFs. For the direct case, the description of the data by the theory is again excellent.

The demonstrated good performance of NLO QCD in describing photoproduction data (especially in the direct regime) gives confidence in the theory, thus rendering possible the extraction of QCD parameters like the strong coupling constant, α_s, or the proton and photon PDFs from the data. One example of the former is given in [5], where a value $\alpha_s(M_Z) = 0.1224 \pm 0.0001(\mathrm{stat.})^{+0.0022}_{-0.0019}(\mathrm{exp.}) \pm^{+0.0054}_{-0.0042}(\mathrm{th.})$ was extracted from an inclusive-jet measurement in photoproduction. Many other precision extractions of α_s, from jet measurements in both DIS and photoproduction, also exist. The impact of jet cross sections in constraining the PDFs is discussed in the next section.

Recently, the symmetry group underlying the strong interaction has been studied by measuring angular correlations in direct-enriched three-jet photoproduction events [6]. Fig. 7 shows the differential cross sections as functions of the angular correlations between the three jets in the final state and the proton-beam direction. The data are compared to LO calculations based on different symmetry groups, illustrating the sensitivity of the data to the colour configuration. While the measured angular correlations are consistent with the prediction of SU(3), they disfavour other symmetry groups such as SU(N) in the limit of large N. The differences between SU(3) and U$(1)^3$ were found to be smaller than the current statistical uncertainties.

1.3 Jets in Photoproduction and the Proton and Photon PDFs

In [4], both the theoretical uncertainties on dijet cross sections and their sensitivity to the gluon density in the photon and the proton have been investigated in great detail. As is highlighted in Fig. 8 (left), for a special choice of kinematics, there are regions in which the proton PDF uncertainty (indicated as the region between the two solid lines) is as large as, or even larger than, the combined theoretical uncertainties due to the choice of renormalization scale, factorization scale,

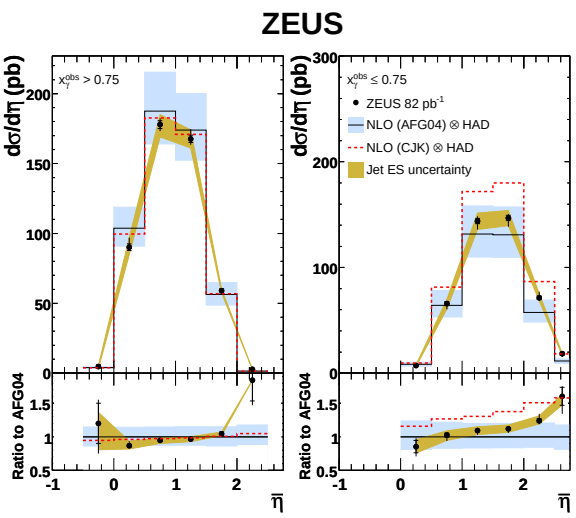

Fig. 5: Photoproduction dijet cross sections as functions of the mean jet pseudorapidity, $\overline{\eta}$, for a direct- and a resolved enriched sample [4].

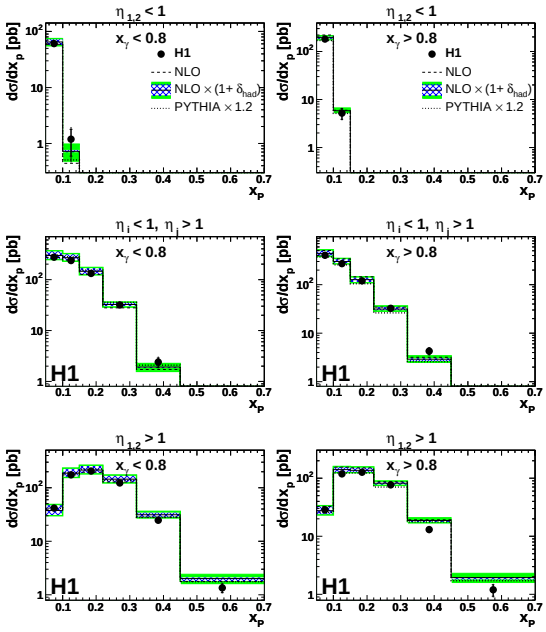

Fig. 6: Photoproduction dijet cross sections as functions of the momentum fraction x_p for a direct- and a resolved enriched sample [1].

α_s, and hadronisation correction. Also, the uncertainty due to the very imprecise knowledge of the photon PDF may be very large, reaching values of up to 60%, as indicated by the dashed line in the figure, which shows the difference in the cross section prediction between two different photon PDF parameterisations. Dijet data do, therefore, have the potential to further constrain both quark and gluon densities in the proton and the photon. This is indicated in Fig. 8 (right), which shows the fraction of gluon-induced events on the proton side (dark dashed line) and on the photon side according to two different photon PDF parameterisations (light dashed and solid lines). The amount of gluon-induced events can be as large as 60%, depending on the detailed kinematics under consideration.

The large discrepancies between different photon PDF parameterisations are also visible in the comparison of NLO QCD predictions with dijet cross sections in the resolved regime, like in Fig. 4 (right) or Fig. 5 (right). For example, in Fig. 4, the resolved dijet cross section can be approximately described by the NLO prediction using the CJK photon PDF parametrization, but not by the AFG04 parametrization, which is off by up to 40–50%. This difference highlights the potential of the data to further constrain the photon PDFs.

A first example of the benefit of jet photoproduction data on determinations of the proton PDFs is given in Figs. 9 and 10. Fig. 9 shows, for an older measurement of photoproduction dijet cross sections [2], the ratio of the measured cross sections over the NLO prediction. An

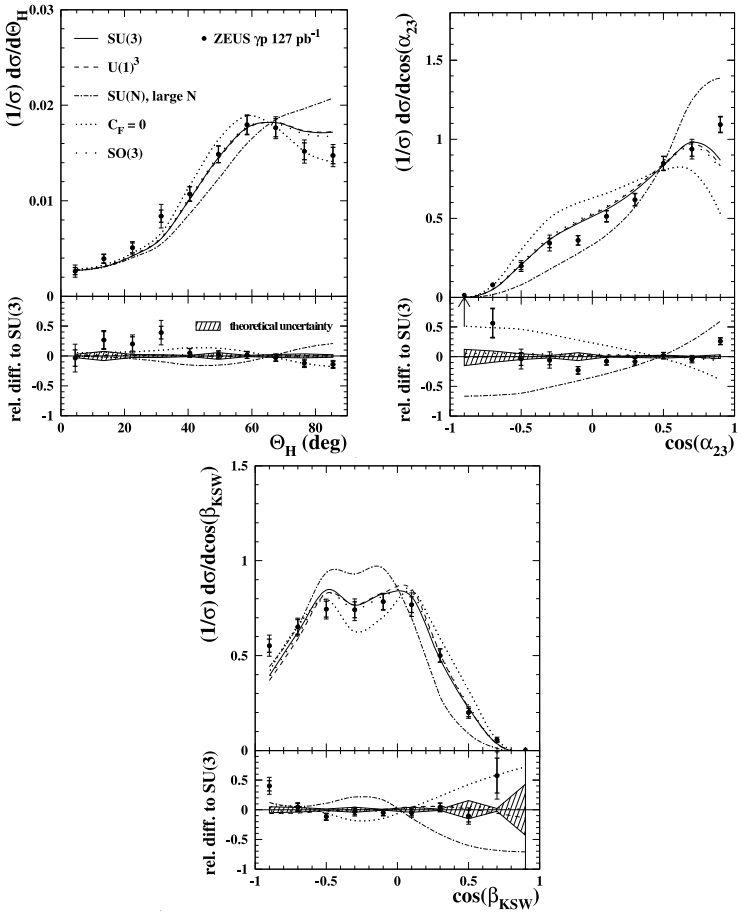

Fig. 7: Photoproduction trijet cross sections as functions of angular correlation between the jets and the proton-beam direction, for a direct enriched sample [6].

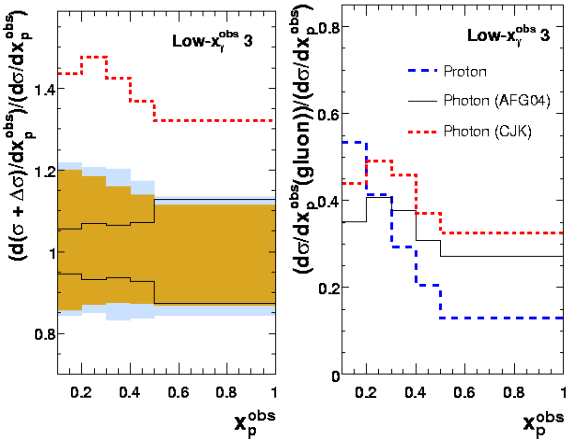

Fig. 8: Left: Theoretical uncertainties on photoproduction dijet cross sections in a special kinematic region [4]. The uncertainties are the total (outer shaded band), that from varying μ_R (inner shaded band), the proton PDF uncertainties from the ZEUS-JETS fit (solid lines) and the difference from using the CJK photon PDF, rather than AFG04 (dashed line). Right: Gluon-induced contributions to photoproduction dijet cross sections in the same kinematic region.

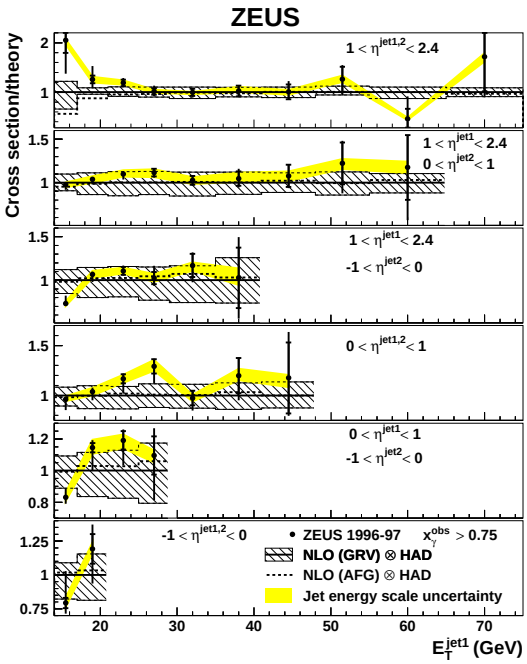

Fig. 9: Ratio of data over NLO QCD predictions for photoproduction dijet events in the direct regime as function of jet transverse energy and pseudorapidity, E_T and η [2].

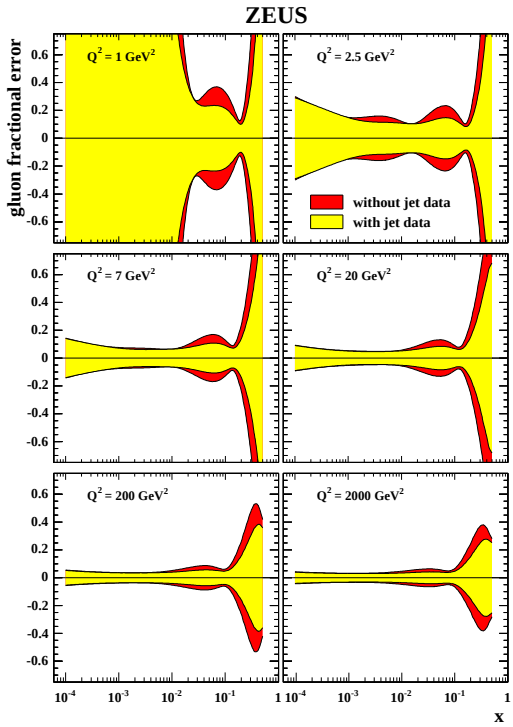

Fig. 10: Improvement of the gluon density by using jet data in NLO QCD fits of the PDFs [7].

overall good description is found, with data and theory in agreement almost everywhere within the combined theoretical and experimental uncertainties. These data (together with data from DIS jet analyses) have been used as additional inputs (besides the usual inclusive F_2 data) to an NLO QCD PDF fit [7]. The success of this fit is demonstrated in Fig. 10, which shows the fractional gluon density uncertainty as a function of the proton momentum fraction x in different regions of Q^2. The uncertainty without the use of jet data is given by the dark shaded area, and the result including jet data is given by the light shaded area. An improvement in the uncertainty of up to 35% is clearly visible, especially in the region of medium-to-high-x values.

The aim now is to further improve the proton PDFs (and here especially the gluon density at high values of x, since this is particularly important for LHC physics) by using more precise measurements or cross sections measured in different kinematic regions, from both photoproduction and DIS. Constraining the photon PDFs will be technically even more demanding, partly because of lack of a consistent PDF error treatment for the photon PDF, and partly because of the increased experimental and theoretical uncertainties for the resolved regime.

1.4 Photoproduction of isolated photons

The production of isolated, or "prompt", photons from the hadronic final state offers an alternative access to the QCD dynamics in ep scattering, with different systematic uncertainties and reduced effects from hadronisation. Isolated photon production has been measured by ZEUS and H1 in both photoproduction [8–10] and DIS [11, 12] . In addition to inclusive measurements of isolated photons, cross sections of photons in association with jets are also often measured, for which there are currently NLO QCD predictions available. In Sec. 2, a detailed description of the latest HERA prompt photon measurement [12] in DIS is presented. Here, only a very brief summary of a recent measurement in photoproduction is given [10].

Fig. 11 [10] shows the photon plus jet cross section, in photoproduction, as a function of E_T^γ and η^γ. The data are compared to NLO QCD calculations (shaded band) and to calculations based on the k_T-factorization approach and unintegrated parton densities (hatched band). The results demonstrate that the k_T-factorization approach gives the closest agreement with the data, especially in the low E_T^γ and forward η^γ regions. The fact that NLO QCD does not describe the data at low values of E_T^γ (or E_T^{jet}) currently precludes the use of the low-transverse-energy data in constraining the PDFs or α_s.

1.5 The underlying event and multi-parton interactions

Resolved photon-proton interactions may, in some respects, be regarded as hadron-hadron collisions, with all the additional features with respect to direct interactions. In particular, it is possible in hadron-hadron collisions to have multiple interactions of pairs of partons (so-called 'multi-parton interactions' or 'MPI'), which may populate the hadronic final state with additional soft or hard jets, or additional energy flow throughout the detector. This effect may alter the final state significantly, making it necessary to model it adequately in the Monte Carlo programs used in the analyses. There exist various MPI model implementations in standard generators, such as HERWIG and PYTHIA, which can be tested against data, or whose parameters can be adjusted to describe the data. Here, some recent examples of multi-parton interaction studies at HERA,

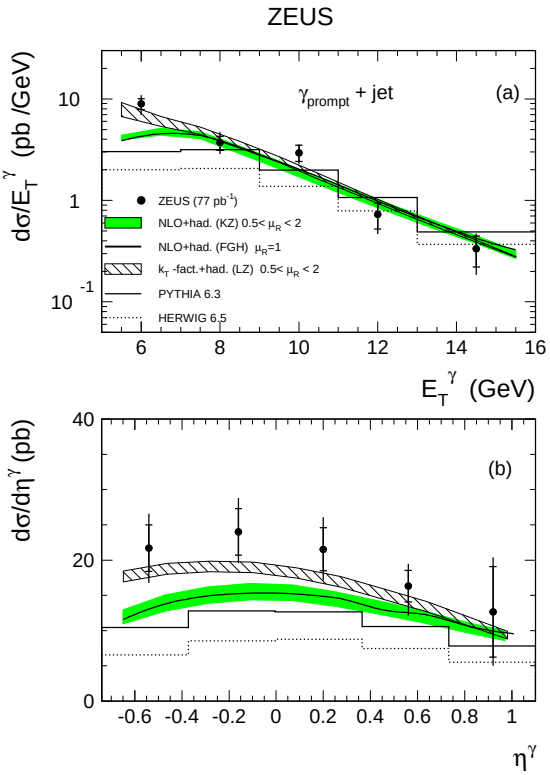

Fig. 11: The $\gamma +$ jet differential cross sections in photoproduction as functions of E_T^γ and η^γ compared to theoretical QCD calculations [10].

from H1 and ZEUS, are briefly reviewed. Note that a more detailed discussion of the H1 results can be found in the WG5 section of these proceedings.

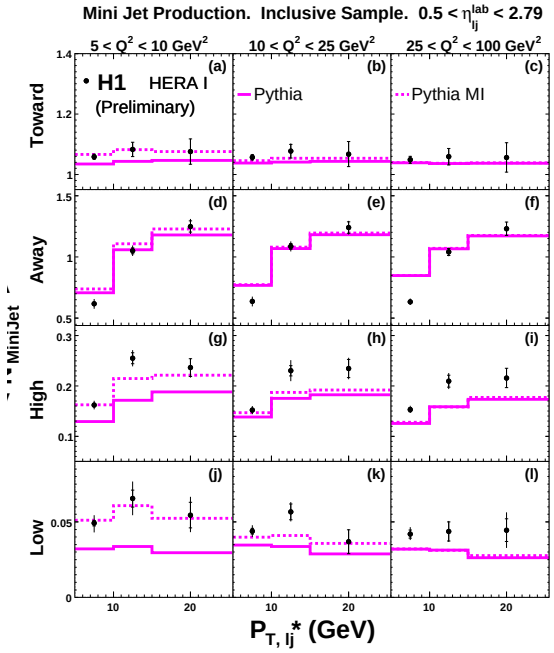

Fig. 12: Mean number of minijets as function of the leading jet p_T [13].

Fig. 12 shows the recent H1 measurement [13] of the mean number of 'minijets' (i.e. soft jets with transverse energies above a very low cut of 3 GeV) in DIS events, with at least one hard jet. The data are shown as a function of this leading jet's transverse momentum, $p^*_{T,lj}$, in different regions of Q^2, and different regions of azimuthal angle with respect to the leading jet's azimuth. The so-called 'Towards' and 'Away' regions are expected to be mostly populated by the results of the first and hardest parton-parton scattering in the event, and the dijet system coming from this scattering should be separated by an azimuthal angle of about π. In contrast, the 'High' and (especially) the 'Low' regions[1], should be particularly sensitive to MPI effects which, in these regions, are not masked out by the harder energy depositions from the leading jet pair. It can be observed that the PYTHIA model with MPI effects switched on ('PYTHIA MI') is in rather good agreement with the data in almost all regions. In contrast, PYTHIA without MPI modelling ('PYTHIA') fails to describe the data in the low Q^2 'High' and 'Low' regions, consistent with the hypothesis of MPI effects dominating in these regions of phase space. Overall, the results indicate that the data strongly favour the models including MPI effects.

Another recent H1 measurement [14], this time of dijets in photoproduction, leads to similar conclusions. Fig. 13 shows the charged particle multiplicity for a resolved-enriched data sample in the 'High' (left) and 'Low' (right) regions as function of the transverse momentum

[1]Note that 'High' and 'Low' refer to the amount of deposited energy in the two regions.

of the leading jet. Again, PYTHIA without MPI modelling ('PYTHIA NMI') does not give a sufficient description of the data while PYTHIA including MPI ('PYTHIA MI') models the data well.

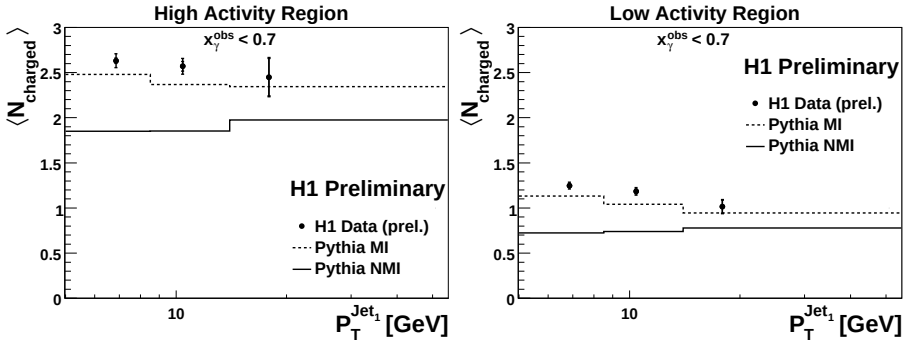

Fig. 13: Charged particle multiplicity for resolved-enriched photoproduction dijets as function of the transverse momentum of the first jet [14].

A similar statement can also derived from a recent measurement of three- and four-jet photoproduction [15] from ZEUS. Fig. 14 shows the four-jet photoproduction cross section as a function of x_γ, and compares it to the predictions of HERWIG and PYTHIA, with and without the inclusion of MPI modelling. The results indicate that the two predictions including MPI effects ('HERWIG+MPI' and 'PYTHIA+MPI') are able to adequately reproduce the data, whereas the models without MPI grossly underestimate the measured cross section in the resolved-enhanced regime (i.e. $x_\gamma < 0.8$). The effect is particularly drastic for low energy scales and low multijet invariant masses, a fact which is illustrated in Fig. 14, where the four-jet mass was required to be between 25 and 50 GeV. It should also be noted that the parameters of the "HERWIG+MPI" model have been tuned to these multijet data, while the "PYTHIA+MPI" parameters have not.

While the HERA measurements clearly favour models in which MPI are included, the data so far do not have the power to specify more precisely the mechanism underlying MPI effects, or to shed light on the energy evolution of MPI effects when going (for example) from TEVATRON to LHC centre-of-mass energies. The models in use so far are rather crude and will have to be replaced by more realistic models and calculations which take correctly into account features like multi-parton exchanges between photon and proton, correlations between these exchanges, etc.

2 Measurement of Isolated Photon Production in Deep Inelastic Scattering at HERA

Author: Katharina Müller

Both the H1 and ZEUS Collaborations have previously measured [8–10] prompt photon cross sections in photoproduction (see, for example, Sec. 1.4). An analysis of the isolated photon cross section in deep inelastic scattering (DIS), with $Q^2 > 35$ GeV^2, has also been published by ZEUS [11]. The present contribution describes the most recent HERA measurement of isolated photon production in DIS ($e + p \rightarrow e + \gamma + X$) from H1.

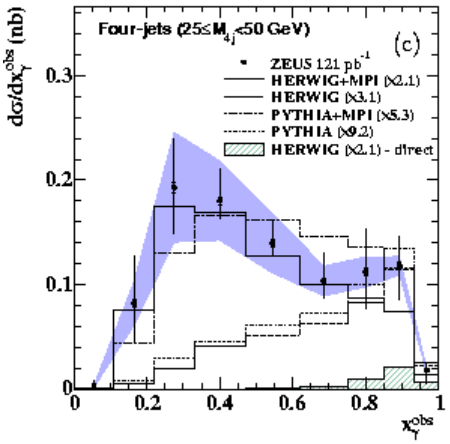

Fig. 14: Photoproduction four-jet cross section as function of x_γ [15].

The measurement of isolated photons in deep inelastic scattering provides a test of QCD in a kinematic range with two hard scales, the four-momentum transfer squared, Q^2, of the exchanged virtual photon and the transverse energy of the emitted photon. In DIS, the final state photon is emitted by a quark (QQ subprocess), by wide angle radiation from the lepton (LL subprocess) or by interference (LQ subprocess). The QQ contribution is dominated by the direct radiation of the photon from the quark involved in the parton level process, but also contains the contribution from quark fragmentation to a photon [16, 17]. Since the photon and the scattered electron are well separated in the present analysis, low angle QED radiation is suppressed. The LL and the more interesting QQ process can not be distinguished experimentally on event basis, but only by comparison with predictions.

The measurement of isolated photons in DIS presented here is based on a total integrated luminosity of 227 pb^{-1}. Full details of the analysis can be found in [12]. Photon candidates with transverse energy $3 < E_T^\gamma < 10$ GeV and pseudorapidity $-1.2 < \eta^\gamma < 1.8$ are selected in DIS events in the kinematic regime $4 < Q^2 < 150$ GeV^2, inelasticity $y > 0.05$ and a mass of the hadronic system $W_X > 50$ GeV. The cut on W_X removes events from elastic compton scattering. The photon candidates are then used together with the other particles in the event, with the exception of the scattered electron, to reconstruct jets using the k_T algorithm [18]. The isolation of the photon is ensured by requiring that it carries at least 90% of the transverse momentum of the jet containing the photon. The isolation criteria removes a large part of the background from decay products of neutral hadrons.

Photons are separated from the remaining neutral hadrons and their decay products by a multivariate analysis of the shapes of the calorimeter energy deposits.

Jet production in events with isolated photons and no additional jet or with at least one jet is also investigated. Hadronic jets are reconstructed for $P_T^{jet} > 2.5$ GeV, the pseudorapidity range is restricted to $-1.0 < \eta^{jet} < 2.1$. All results are compared to a leading order (LO), $\mathcal{O}(\alpha^3\alpha_s^0)$, calculation [19, 20]. The cross sections for a photon plus at least one jet are further

compared to a NLO, $\mathcal{O}(\alpha^3\alpha_s^1)$, calculation [21].

Differential cross sections $d\sigma/d\eta^\gamma$ and $d\sigma/dQ^2$ for the inclusive isolated photon cross section are shown in Fig. 15. Fig. 16 shows the differential cross sections $d\sigma/d\eta^\gamma$ for isolated photons with no additional hadronic jet (a) and with hadronic jets (b). The uncertainty on the shower description gives the dominant contribution to the systematical error. The cross sections are shown together with the predictions by the LO calculation. A comparison to a NLO calculation is possible for the photon plus jets cross section. The calculations are corrected to hadron level. The corrections amount to, at most, -30%.

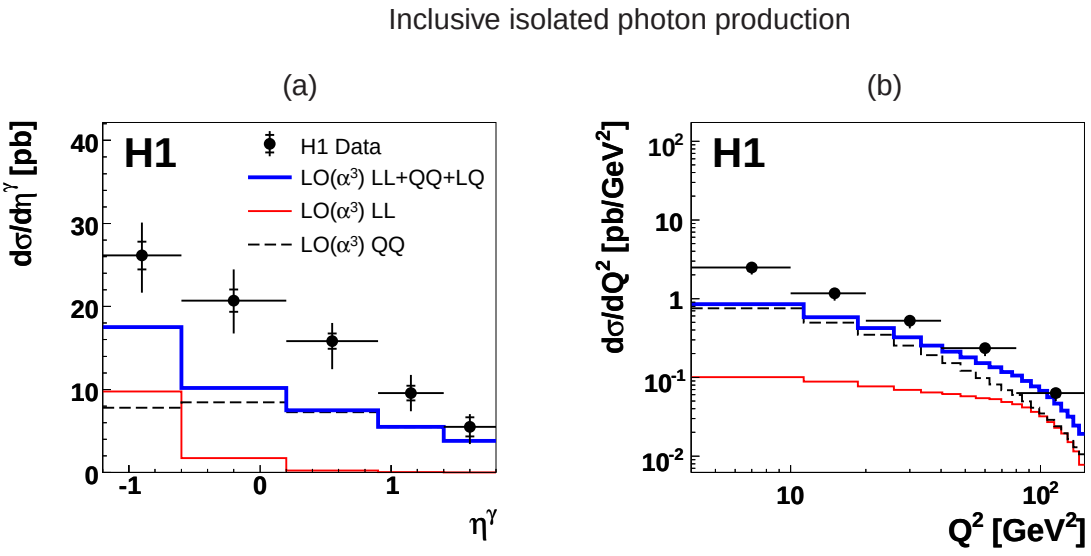

Fig. 15: Inclusive differential isolated photon cross sections $d\sigma/d\eta^\gamma$ (a), $d\sigma/dQ^2$ (b) for $3 < E_T^\gamma < 10$ GeV, $-1.2 < \eta^\gamma < 1.8$, $W_X^2 > 2500$ GeV^2 and $4 < Q^2 < 150$ GeV^2. The inner error bars on the data points indicate the statistical error, the full error bars contain in addition the systematic errors added in quadrature. The cross sections are shown together with a leading order, $\alpha^3\alpha_s^0$, calculation [20] corrected for hadronisation effects, LL corresponding to radiation from the electron and QQ to radiation from the quark.

The LO $\mathcal{O}(\alpha^3\alpha_s^0)$ calculation underestimates the inclusive cross sections by roughly a factor of two, most significantly at low Q^2. The relative contribution of radiation from the electron (LL) and the quark(QQ) depends strongly on η^γ and Q^2. At high and medium η^γ and low Q^2, radiation by the quark dominates. The shapes of the $d\sigma/dE_T^\gamma$ and $d\sigma/d\eta^\gamma$ distributions are described reasonably well. The comparison of data to the LO calculation in bins of η^γ show that the difference in normalisation can mainly be attributed to an underestimation of the QQ contribution [12].

The LO prediction also underestimates the production of isolated photons plus no hadronic jet and photons plus jets by a similar factor as for the inclusive measurement. The NLO $\mathcal{O}(\alpha^3\alpha_s^1)$

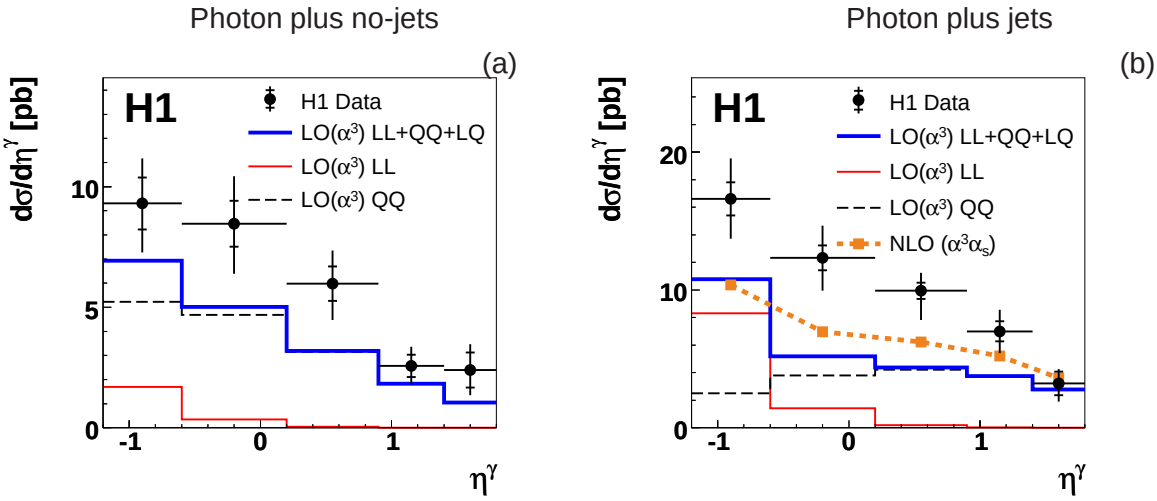

Fig. 16: Differential cross sections $d\sigma/d\eta^{\gamma}$ for photon plus no-jets (a) and photon plus jets (b), with $P_T^{jet} > 2.5$ GeV and $-1.0 < \eta^{jet} < 2.1$. The cross sections are compared to a leading order, $\mathcal{O}(\alpha^3\alpha_s^0)$, calculation [19] as in Figure 1. The photon plus jet sample is additionally compared to a NLO ($\alpha^3\alpha_s$) calculation [21]. The bin averaged NLO cross sections are indicated by the squares.

prediction for photon plus jet is higher than the LO prediction, most significantly at low Q^2, but still underestimates the data. The NLO calculation describes the shapes of the differential cross sections reasonably well.

The LL contribution is largely suppressed for the sample with no additional jet due to the cut on W_X. The cross section for photon plus jet production is roughly two times higher than for photon plus no additional jet. This is in contrast to the inclusive $ep \to eX$ cross section, where topologies with an additional jet are suppressed by $\mathcal{O}(\alpha_s)$. The similar cross sections for photon events with or without additional jets may be explained by the fact that both topologies correspond to the same order $\mathcal{O}(\alpha_s^0)$ in perturbative QCD. [20] The cross section for photon plus jet production is roughly two times higher than for photon plus no-jets.

At leading order $\mathcal{O}(\alpha_s^0)$, the quark fragmentation contribution to the cross section enters only the sample with a photon and no hadronic jet [20]. Hence, the observed excess of the data can not solely be attributed to an underestimation of that contribution.

Further theoretical investigations are needed to understand the observed discrepancy between the measurements and the predictions, including for instance the calculation of higher order processes.

References

[1] H1 Collaboration, A. Aktas *et al.*, Phys. Lett. **B639**, 21 (2006), arXiv:hep-ex/0603014.

[2] ZEUS Collaboration, S. Chekanov *et al.*, Eur. Phys. J. **C23**, 615 (2002), arXiv:hep-ex/0112029.

[3] ZEUS Collaboration, S. Chekanov *et al.*, Eur. Phys. J. **C35**, 487 (2004), arXiv:hep-ex/0404033.

[4] ZEUS Collaboration, S. Chekanov *et al.*, Phys. Rev. **D76**, 072011 (2007), arXiv:0706.3809 [hep-ex].

[5] ZEUS Collaboration, S. Chekanov *et al.*, Phys. Lett. **B560**, 7 (2003), arXiv:hep-ex/0212064.

[6] ZEUS Collaboration, . S. Chekanov (2008), arXiv:0808.3783 [hep-ex].

[7] ZEUS Collaboration, S. Chekanov *et al.*, Eur. Phys. J. **C42**, 1 (2005), arXiv:hep-ph/0503274.

[8] ZEUS Collaboration, J. Breitweg *et al.*, Phys. Lett. **B472**, 175 (2000), arXiv:hep-ex/9910045.

[9] H1 Collaboration, A. Aktas *et al.*, Eur. Phys. J. **C38**, 437 (2005), arXiv:hep-ex/0407018.

[10] ZEUS Collaboration, S. Chekanov *et al.*, Eur. Phys. J. **C49**, 511 (2007), arXiv:hep-ex/0608028.

[11] ZEUS Collaboration, S. Chekanov *et al.*, Phys. Lett. **B595**, 86 (2004), arXiv:hep-ex/0402019.

[12] H1 Collaboration, F. D. Aaron *et al.*, Eur. Phys. J. **C54**, 371 (2008), arXiv:0711.4578 [hep-ex].

[13] H. Collaboration, *Minijet Production in Deep Inelastic Scattering at HERA* (unpublished). H1-PRELIM-07-032.

[14] H. Collaboration, *Study of multiple interactions in photoproduction at HERA* (unpublished). H1-PRELIM-08-036.

[15] ZEUS Collaboration, S. Chekanov *et al.*, Nucl. Phys. **B792**, 1 (2008), arXiv:0707.3749 [hep-ex].

[16] K. K. *et al.*, Z. Phys. C **6**, 131 (1980).

[17] M. Gluck, L. E. Gordon, E. Reya, and W. Vogelsang, Phys. Rev. Lett. **73**, 388 (1994).

[18] S. D. Ellis and D. E. Soper, Phys. Rev. **D48**, 3160 (1993), arXiv:hep-ph/9305266.

[19] A. Gehrmann-De Ridder, T. Gehrmann, and E. Poulsen, Phys. Rev. Lett. **96**, 132002 (2006), arXiv:hep-ph/0601073.

[20] A. Gehrmann-De Ridder, T. Gehrmann, and E. Poulsen, Eur. Phys. J. **C47**, 395 (2006), arXiv:hep-ph/0604030.

[21] A. Gehrmann-De Ridder, G. Kramer, and H. Spiesberger, Nucl. Phys. **B578**, 326 (2000), arXiv:hep-ph/0003082.